D. W. Apley
Department of Industrial Engineering,
Texas A&M University,
College Station, TX 77843-3131
apley@ie.tamu.edu

J. Shi
Department of Industrial and
Operations Engineering,
The University of Michigan,
Ann Arbor, MI 48109-2117
shihang@engin.umich.edu

Diagnosis of Multiple Fixture Faults in Panel Assembly

This paper presents a modeling procedure and diagnostic algorithm for fixture related faults in panel assembly. From geometric information about the panel and fixture, a fixture fault model can be constructed off-line. Combining the fault model with in-line panel dimensional measurements, the algorithm is capable of detecting and classifying multiple fixture faults. The algorithm, which relies heavily on the fault model, is based on least squares estimation. Consequently, the test is of relatively simple form and is easily implemented and analyzed. Experimental results of applying the algorithm to an autobody assemble process are provided.

1 Introduction

Panel assembly is an integral part of many manufacturing processes, such as the assembly of automobile bodies, office furniture, and home appliances (e.g., washers and dryers). The dimensional quality of the completed product is highly dependent on the level of accuracy with which the panels were fixtured. Consequently, design and maintenance of accurate fixturing is an important research area.

In the past decade, there has been large amount of research concerning automated fixture design and analysis. The problems are usually formulated as constrained optimization problems satisfying the fixturing requirements (Asada and By, 1985; Chou, et al., 1989; Menassa and DeVries, 1991) of (1) uniqueness of the workpiece location; (2) accessibility to and detachability of the workpiece; (3) clamping stability; (4) positioning stability; and (5) total restraint in the presence of any external forces. Asada and By (1985) use a kinematic analysis to develop conditions for ensuring that the fixture uniquely locate the workpiece and that one is able to insert (accessibility) and remove (detachability) the workpiece from the fixture. Chou et al. (1989) use screw theory to ensure that none of the reaction forces exerted on the workpiece by the locating elements become negative during positioning (positioning stability), clamping (clamping stability), and subsequent machining (total restraint). Menassa and DeVries (1991), using finite element analysis, optimize the position of the support blocks to minimize workpiece deflection due to applied forces. Rong and Zhu (1992) develop a search and retrieve (over a set of existing fixture designs) technique with kinematic requirement considerations. Hockenberger and De Meter (1995) and De Meter (1995) conduct an experimental analysis into the causes of workpiece deflection under machining forces and optimize the layout of clamps and locators using a mini-max locating force criteria with kinematic and total restraint constraints. King and Hutter (1993) combine kinematic and total restraint requirements into an overall optimization criteria, including frictional forces in their model.

While these works represents significant contributions to fixturing research, they are all geared towards fixture design. No matter how good the fixture design is and how well laid out the locating pins and blocks are, over time the locating elements may become worn, loose, bent, or broken. The impact of this could be a severe deterioration in the ability of the fixture to accurately locate the panel. In fact, studies have concluded that fixture faults are the major root cause of autobody dimensional variation (ABC, 1993) and that at one domestic automobile assembly plant 72 percent of all root causes of dimensional variation over an 18 month period were due to fixture failures (Ceglarek et al., 1994).

In light of this, a method for detecting and diagnosing fixture failures, based on in-line panel measurements, would be highly advantageous. In spite of the prevalent research on fixture design, research on fixture diagnosis is scarce. The most likely reason for this was the past difficulties in obtaining sufficient dimensional measurements. However, given the recent development and implementation of Optical Coordinate Measuring Machines (OCMMs), especially in the automotive industry, new opportunities for fixture failure diagnosis have emerged. OCMMs are typically installed at the end of major autobody subassemblies and provide a 100 percent inspection rate with up to 150 measurement points on each subassembly.

A few recent works have taken advantage of OCMM technology and developed methods for diagnosing dimensional variation problems in autobody assembly. Hu and Wu (1992) developed a method based on the multivariate statistical technique known as Principle Components Analysis (PCA). The method relies on an intuitive interpretation of the principle components to gain insight into the root causes of dimensional variation. Ceglarek et al. (1994) developed a rule-based approach for identifying failing subassembly stations. By restricting attention to fixture-related problems, Ceglarek and Shi (1996) developed a PCA-based diagnostic approach that has achieved considerable success in autobody assembly implementations. The class of fixture related problems their method applies to are those resulting from worn, loose, or broken locating elements.

The method of Ceglarek and Shi (1996), however, has two significant drawbacks. Firstly, it cannot detect multiple fixture faults. In fact, if two or more faults occur simultaneously with similar severity, then their method produces erroneous results and is likely to miss both faults. Secondly, the statistics of their test are intractible, meaning that it is impossible to analyze the test performance theoretically. Thus, there is no efficient means of choosing a test threshold to guarantee a desired probability of false alarm, other than through extensive simulation and/or experience.

The objective of this research is to develop a diagnostic algorithm for detecting and classifying fixture faults in panel assembly operations that (1) applies to multiple fixture faults occurring simultaneously, and (2) has detection and false alarm properties that are easily determined theoretically. One result of (2) is that all test parameters (e.g. the threshold) can easily be selected to provide a desired probability of false alarm. By fixture-related faults it is meant worn, loose, or broken locating elements. An additional contribution of this research is the development of a model that relates fixture faults to the displacement of measured points on the panel. The model is essential to the development of the diagnostic algorithm and, in general,

Contributed by the Manufacturing Engineering Division for publication in the JOURNAL OF MANUFACTURING SCIENCE AND ENGINEERING. Manuscript received May 1996; revised Aug. 1996. Associate Technical Editor: C. H. Meng.

allows a convenient means of interpreting and analyzing the fixture faults considered.

The overall procedure for implementing the algorithm is illustrated in Fig. 1.1. Based only on the panel geometry (CAD Data) and fixture geometry (Fixture Layout Knowledge) the fixture fault model is constructed off-line. To implement the algorithm, the model is merged with in-line OCMM panel measurement data. The diagnostic algorithm, based on least squares estimation theory, then uses the model and in-line data to detect and classify multiple fixture faults.

The remainder of the paper is summarized as follows. In section 2 the fixture fault model is presented and illustrated with an example. Section 3 develops the least squares based diagnostic algorithm, and section 4 theoretically analyzes the algorithm performance in terms of the probability of detecting the faults and the probability of false alarm. Section 5 presents experimental results in which the algorithm was applied to fixture fault detection in autobody panel assembly. Conclusions and discussion follow in section 6.

2 A Linear Model For Fixture Related Variation

Consider the fixturing of the flat rigid body panel illustrated in Fig. 2.1, which follows the 3-2-1 fixturing principle. The three shaded blocks constrain the motion of the panel in the y direction, and the combination pin/hole (P_1) and pin/slot (P_2) constrain the motion in the x-z plane. Together, the combination of tooling elements (blocks and pins) constrains all six degrees-of-freedom of the rigid panel. In this section, we develop a linear model relating small displacements of the tooling elements to the overall displacement of (measured points on) the panel. Such panel displacements commonly occur in panel assembly, the result of worn, loose, or broken tooling elements. Although we illustrate the concepts with the simple setup of Fig. 2.1, the model will be applicable to generic 3-2-1 rigid body fixturing. The model will also apply to n-2-1 nonrigid body fixturing if the faults being considered cause panel motion only in the plane of rigidity. For example, if the panel in Fig. 2.1 is non rigid in the y direction (and, thus, requires n locating blocks to constrain motion in the y direction) but rigid in the x-z plane, then the model will apply to faults which cause motion only within the x-z plane.

First consider the effects of pin displacements on the panel position, which, since the panel is flat, only cause motion in the x-z plane. This situation is illustrated in Fig. 2.2. Suppose the x-y-z coordinates of three points $M_1 = (M_1(x), M_1(y), M_1(z))$, $M_2 = (M_2(x), M_2(y), M_2(z))$, and $M_3 = (M_3(x), M_3(y), M_3(z))$ are to be measured. Let $\mathbf{x} \equiv [M_1(x)M_1(y)M_1(z)M_2(x)M_2(y)M_2(z)M_3(x)M_3(y)M_3(z)]^T$ be the 9-dimensional measurement vector consisting of all components of the measurement points. The immediate goal is to find the effects of positional displacements of the pins on $\mathbf{x}$. The displacement of P_2 in the x direction has no effect on $\mathbf{x}$, provided the pin does not displace further than the boundary of the slot. Let $\delta P_2(z)$ denote the displacement of P_2 in the z direction, $\delta P_1(x)$ and $\delta P_1(z)$ be defined similarly, and $\delta\mathbf{x}$ denote the resulting deviation (from nominal) of the measurement vector $\mathbf{x}$.

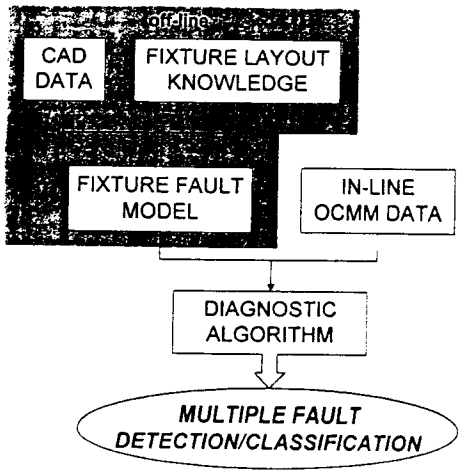

Fig. 1.1 Outline of the fixture fault diagnosis method

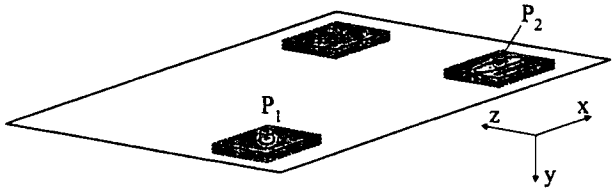

Fig. 2.1 Illustration of the 3-2-1 fixturing principle for rigid panels

The exact relationship between $\delta\mathbf{x}$ and $\delta P_1(x)$, $\delta P_1(z)$, and $\delta P_2(z)$ can be expressed as some nonlinear function $\mathbf{f}$ which depends on the geometry of the panel, i.e. $\delta\mathbf{x} = \mathbf{f}(\delta P_1(x), \delta P_1(z), \delta P_2(z))$. To determine the exact effect of any of the pin displacements, all of the pin displacements must be considered simultaneously. Specifically, the effect of $\delta P_2(z)$ will depend also on $\delta P_1(x)$ and $\delta P_1(z)$. However, it is assumed that all of the pin displacements are small relative to the overall dimensions of the panel. Consequently, the higher order terms of a Taylor expansion of $\mathbf{f}$ can be neglected, resulting in the linearized relationship

$$\delta\mathbf{x} \cong \left[\frac{\partial \mathbf{f}}{\partial P_2(z)}\right]\delta P_2(z) + \left[\frac{\partial \mathbf{f}}{\partial P_1(x)}\right]\delta P_1(x) + \left[\frac{\partial \mathbf{f}}{\partial P_1(z)}\right]\delta P_1(z),$$

where the partial derivatives are evaluated at $\delta P_1(x) = \delta P_1(z) = \delta P_2(z) = 0$ (i.e., the nominal position of the pins). In this linearized relationship the effect of a P_2 displacement does not depend on how much P_1 deviates from nominal, and vice-versa, since the partial derivatives are evaluated at the nominal positions of the pins. Thus, the most straightforward way to calculate the effect of, say, $\delta P_2(z)$ is to determine how the panel moves with $\delta P_1(x) = \delta P_1(z) = 0$. The same can be done for the P_1 displacements, and the effects of all three faults together are additive.

The net effect of a displacement $\delta P_2(z)$ is to cause the panel to rotate about P_1, as illustrated in Fig. 2.3. From simple geometric arguments it follows that the effect of a small $\delta P_2(z)$ can be expressed as

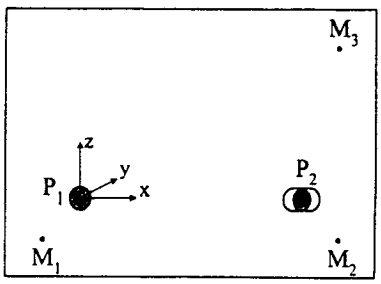

Fig. 2.2 Illustration of panel fixturing in the x-z plane

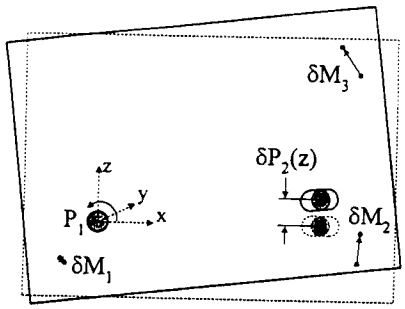

Fig. 2.3 Illustration of the effect of a z direction displacement of P_2: a rotation about P_1

$$\delta \mathbf{x} \cong \mathbf{c}_1 \delta P_2(z),$$

where

$$\mathbf{c}_1 \equiv \frac{1}{P_2(x)} [-M_1(z) \quad 0 \quad M_1(x) \quad -M_2(z) \quad 0 \quad M_2(x) \quad -M_3(z) \quad 0 \quad M_3(x)]^T.$$

The quantities in the expression for $\mathbf{c}_1$ are the nominal coordinates of the measurement points, and $P_2(x)$ denotes the nominal x-coordinate of P_2. The origin of the coordinate system has been chosen to coincide with the nominal position of P_1. Note that if one were to determine the exact nonlinear relationship $\mathbf{f}$ referred to in the preceeding paragraph, its partial derivative with respect to $\delta P_2(z)$, evaluated at the nominal position, would equal $\mathbf{c}_1$.

Likewise, the displacements due to small $\delta P_1(x)$ and $\delta P_1(z)$ are

$$\delta \mathbf{x} \cong \mathbf{c}_2 \delta P_1(x),$$

and

$$\delta \mathbf{x} \cong \mathbf{c}_3 \delta P_1(z),$$

respectively, where

$$\mathbf{c}_2 \equiv [1\ 0\ 0\ 1\ 0\ 0\ 1\ 0\ 0]^T,$$

and

$$\mathbf{c}_3 \equiv \frac{1}{P_2(x)} [M_1(z) \quad 0 \quad (P_2(x) - M_1(x)) \quad M_2(z) \quad 0 \quad (P_2(x) - M_2(x)) \quad M_3(z) \quad 0 \quad (P_2(x) - M_3(x))]^T.$$

All quantities in the expression for $\mathbf{c}_3$ are nominal coordinates. Since in the linearized model the effects of the faults are additive, it follows that if all three pin displacements are present,

$$\delta \mathbf{x} \cong \mathbf{c}_1 \delta P_2(z) + \mathbf{c}_2 \delta P_1(x) + \mathbf{c}_3 \delta P_1(z) = \mathbf{C}\mathbf{v}, \tag{2.1}$$

where $\mathbf{C} \equiv [\mathbf{c}_1\ \mathbf{c}_2\ \mathbf{c}_3]$ and $\mathbf{v} \equiv [\delta P_2(z)\ \delta P_1(x)\ \delta P_1(z)]^T$. Note that the development of (2.1) implied an actual pin displacement, which would result from, for example, a loose or broken pin. If instead the pin is worn, so that there is some clearance between the pin and hole/slot, the effects would be identical to those of a loose pin even though the pin is not actually displacing. Consequently, a worn tooling element will be treated as a tooling element displacement also.

In a similar manner, one can also consider the effects of block displacements on the panel motion. Since the panel is assumed flat, small displacements of the blocks in the x-z plane have no effect on the position of the panel. In general, small block displacements in the x-z plane will not affect the position of the panel provided the vector normal to the panel surface, at the point of contact with the block, is orthogonal to the x-z plane.

Enumerate the three blocks as B_1, B_2, and B_3. Let $l_{1,2}$ denote the imaginary line connecting (the nominal position of) blocks 1 and 2, and let $l_{1,3}$ and $l_{2,3}$ be defined similarly. Define $d(B_i, l_{j,k})$ to be the nominal distance between block i and line $l_{j,k}$, and define $d(M_i, l_{j,k})$ to be the nominal distance between measurement point M_i and line $l_{j,k}$. Define the y-direction displacements of blocks 1 through 3 as $\delta B_1(y)$, $\delta B_2(y)$, and $\delta B_3(y)$.

Since a displacement of any of the three blocks in the y direction causes a rotation of the panel about the line connecting the other two blocks, it follows that the effects of the three block displacements on the measured points are given by

$$\delta \mathbf{x} \cong \mathbf{c}_4 \delta B_1(y) + \mathbf{c}_5 \delta B_2(y) + \mathbf{c}_6 \delta B_3(y),$$

where

$$\mathbf{c}_4 \equiv \frac{1}{d(B_1, l_{2,3})} [0 \quad \pm d(M_1, l_{2,3}) \quad 0 \quad 0 \quad \pm d(M_2, l_{2,3}) \quad 0 \quad 0 \quad \pm d(M_3, l_{2,3}) \quad 0]^T,$$

$$\mathbf{c}_5 \equiv \frac{1}{d(B_2, l_{1,3})} [0 \quad \pm d(M_1, l_{1,3}) \quad 0 \quad 0 \quad \pm d(M_2, l_{1,3}) \quad 0 \quad 0 \quad \pm d(M_3, l_{1,3}) \quad 0]^T,$$

and

$$\mathbf{c}_6 \equiv \frac{1}{d(B_3, l_{1,2})} [0 \quad \pm d(M_1, l_{1,2}) \quad 0 \quad 0 \quad \pm d(M_2, l_{1,2}) \quad 0 \quad 0 \quad \pm d(M_3, l_{1,2}) \quad 0]^T.$$

The "$\pm$" symbol indicates that either a positive or a negative sign should precede each element, which can easily be determined given the position of the measurement point relative to the blocks. If faults due to block displacements are also to be included in the model, the $\mathbf{C}$ matrix in (2.1) is augmented to include $\mathbf{c}_4$, $\mathbf{c}_5$, and $\mathbf{c}_6$ as the last three columns, and $\mathbf{v}$ is similarly augmented.

The example used to illustrate the construction of the $\mathbf{C}$ matrix is a special case of the 3-2-1 fixturing principle, commonly used for thin panels, where pins and holes/slots are used to constrain the x-z plane motion. A 3-2-1 method in which six blocks and no pins are used is also common, especially with thicker panels. The preceding example was further specialized in the sense that the panel was flat and rectangular. For arbitrarily shaped panels and 3-2-1 fixturing using six blocks, calculating the panel motion due to block displacements can be much more involved. In general, the panel motion depends on the layout of the locating elements and also on the local surface geometry of the panel in neighborhoods of each point where the locating elements contact the panel (Rong et al., 1995).

Implementation of the fault detection algorithm requires a linearized model relating the locating element displacements to $\delta \mathbf{x}$, as in (2.1). For the small tooling element displacements encountered in practice, a linearized approximation is usually close to the exact relationship. For an arbitrary 3-2-1 fixturing scheme, the first step is to determine the functional form of $\mathbf{f}$ in the nonlinear relationship $\delta \mathbf{x} = \mathbf{f}(\mathbf{v})$. Refer to Rong et al. (1995) for details. As previously discussed, the fact that $\mathbf{f}$ will subsequently be linearized enables one to separately determine the effects of the displacements of each locating element. In general, the $\mathbf{C}$ matrix can then be obtained via $\mathbf{C} \equiv (\partial f / \partial \mathbf{v})$, where $(\partial f / \partial \mathbf{v})$ is the Jacobian matrix such that the ith row, jth column element is $(\partial \mathbf{x}_i / \partial \mathbf{v}_j)$. Here, $\mathbf{x}_i$ is the ith element of $\mathbf{x}$, and $\mathbf{v}_j$ is the jth element of $\mathbf{v}$. The $\mathbf{C}$ matrix depends only on the nominal geometry of the panel and fixture layout and, thus, can be constructed off-line using product/process design information.

After obtaining the $\mathbf{C}$ matrix for a general 3-2-1 fixturing situation, the linearized fault model can be expressed similarly to (2.1) as

$$\mathbf{x}(j) = \mathbf{C}\mathbf{v}(j) + \mathbf{w}(j) \quad j = 1, 2, \ldots, N, \qquad (2.2)$$

where the notation is as follows. Let p denote the number of faults to be modeled, and let n denote the total number of measurements taken on each panel. For the situation in Fig. 2.2, $p = 3$ (x and z displacement of P_1 and z displacement of P_2) and $n = 9$ (x-y-z coordinates of three measurement points). $\mathbf{x}(j)$ denotes the n-dimensional vector of measurements on the jth panel. The index j can be thought of as a "time" index. For example, if the panels represent a particular component of an autobody, then j denotes the car number. N denotes the total number of panels being measured. For simplicity, the elements of $\mathbf{x}(\cdot)$ will be deviations from nominal, what was previously referred to as $\delta\mathbf{x}$. $\mathbf{v}(j)$ denotes the p-dimensional vector, the ith component of which characterizes the ith fault, as it occurs on the jth panel. Thus, for the Fig. 2.2 example $\mathbf{v}(j) = [\delta P_2(z)\ \delta P_1(x)\ \delta P_1(z)]^T$ at the time of the jth panel. Let $\{\mathbf{c}_i\}_{i=1}^p$ be n-dimensional column vectors such that $\mathbf{c}_i$ defines the linear or linearized effect of the ith fault on the measurement vector $\mathbf{x}(\cdot)$. Then $\mathbf{C}$ is defined as $\mathbf{C} \equiv [\mathbf{c}_1\ \mathbf{c}_2 \ldots \mathbf{c}_p]$. $\mathbf{w}(j)$ is the n-dimensional "noise" vector that represents any discrepancy between the modeled effects of the faults and what is actually measured on the jth panel. $\mathbf{w}(\cdot)$ can be thought of as the aggregated effects of sensor noise and any inherent unmodeled variation in the manufacturing process.

We make the following assumptions regarding the model:

(A1) $\{\mathbf{v}(j)\}_{j=1}^N$ are random vectors that follow a multivariate Gaussian distribution with zero mean and $p \times p$ covariance matrix $\mathbf{K}_v \equiv E[\mathbf{v}(\cdot)\mathbf{v}^T(\cdot)]$, denoted $\mathbf{v}(\cdot) \sim N(\mathbf{0}, \mathbf{K}_v)$. Here, $E[\cdot]$ denotes the probabilistic expectation. Furthermore, assume $\mathbf{v}(j)$ is uncorrelated with $\mathbf{v}(i)$ for $i \neq j$.

(A2) The columns of $\mathbf{C}$ are linearly independent. In general, if a sufficient number of measurements are taken this will be the case. Since $\mathbf{C}$ is an $n \times p$ matrix, an absolute minimum is $n \geq p$. Also, let each column of $\mathbf{C}$ be scaled so as to have unit norm. The elements of $\mathbf{v}(\cdot)$ must be rescaled accordingly.

(A3) $\{\mathbf{w}(j)\}_{j=1}^N$ are zero-mean Gaussian random vectors, i.e. $\mathbf{w}(\cdot) \sim N(\mathbf{0}, \mathbf{K}_w)$, where $\mathbf{K}_w = \sigma_w^2\mathbf{I}$ and $\mathbf{I}$ is the $n \times n$ identity matrix. Furthermore, assume $\mathbf{w}(j)$ is uncorrelated with $\mathbf{w}(i)$ for $i \neq j$, and $\mathbf{w}(j)$ is uncorrelated with $\mathbf{v}(i)$ for all i and j.

Some comments are in order regarding the assumptions. (A1) essentially says that the types of faults being considered are *variation* sources, as opposed to faults that manifest themselves as mean shifts. For example, a P_2 fault in Fig. 2.2, resulting from a worn or loose pin, would cause the panels to rotate randomly about P_1, with some panels rotating in a clockwise direction and some in a counter-clockwise direction. The average rotation is zero since $\mathbf{v}(\cdot)$ is assumed zero-mean, and the average "magnitude" of the rotation is determined by the variance of the corresponding element of $\mathbf{v}(\cdot)$. Faults that are not manifested as variation, but rather as mean shifts (e.g. a bent or mislocated pin), can still be modeled by (2.2) if the zero-mean assumption on $\mathbf{v}(\cdot)$ is dropped. Much of the analysis of the detection algorithm developed in the subsequent section applies to variation type faults and does not apply directly to mean shift faults. However, if mean shift type faults or both mean shift and variation type faults are occurring, the developed algorithm can still be successfully applied. How to interpret the algorithm in this situation is addressed as Remark 3 in section 3.1.

In (A3) the assumption that $\mathbf{K}_w = \sigma_w^2\mathbf{I}$ means that the noise affecting the measurements are uncorrelated and of equal variance. This can be assumed without loss of generality if the true $\mathbf{K}_w$ is known or can be estimated from data during which none of the faults were present. In this event, the measurement vectors $\mathbf{x}(\cdot)$ must be transformed by $\mathbf{K}_w^{-1/2}$ before applying the algorithm. Premultiplying (2.2) by $\mathbf{K}_w^{-1/2}$ gives

$$\mathbf{x}'(j) = \mathbf{C}'\mathbf{v}(j) + \mathbf{w}'(j),$$

where $\mathbf{x}'(j) \equiv \mathbf{K}_w^{-1/2}\mathbf{x}(j)$, $\mathbf{C}' \equiv \mathbf{K}_w^{-1/2}\mathbf{C}$, and $\mathbf{w}'(j) \equiv \mathbf{K}_w^{-1/2}\mathbf{w}(j) \sim N(\mathbf{0}, \mathbf{I})$. (A3) then applies to $\mathbf{w}'(\cdot)$, and the algorithm can be applied to the transformed measurements $\mathbf{x}'(\cdot)$ instead of $\mathbf{x}(\cdot)$.

3 An Algorithm for Fault Detection and Classification

In this section a least squares based algorithm is developed for detecting and classifying multiple faults in panel assembly. The type of faults the algorithm is applicable to are the variation-related faults described by the model (2.2) under assumptions (A1)–(A3). The most typical causes of such faults are worn, loose, or broken locating elements. As discussed in the paragraphs following the assumptions, (A1) and (A3) are not overly restrictive and can often be worked around.

3.1 Algorithm Development. The physical reasoning behind the algorithm is as follows. Let $\{\sigma_i^2\}_{i=1}^p$ denote the diagonal elements of $\mathbf{K}_v$. If $\mathbf{v}_i(\cdot)$ denotes the ith element of $\mathbf{v}(\cdot)$, then σ_i^2 is the variance of $\mathbf{v}_i(\cdot)$. Thus, σ_i^2 is in some sense a measure of the severity of the ith fault. $\sigma_i^2 = 0$ means that $\mathbf{v}_i(j) = 0$ for all j or, in other words, the ith fault is not present. On the other hand, if σ_i^2 is large, the ith fault is present and quite severe. Consequently, we will refer to σ_i^2 as the magnitude of the ith fault.

This interpretation suggests a method of determining whether each of the p faults are present: From the measurement data and the model (2.2), estimate $\{\sigma_i^2\}_{i=1}^p$. If the estimated magnitude of one or more of the faults is large in some sense, then conclude that those faults are present. Note that the estimate of σ_i^2 also provides a measure of how severe the fault is. The remainder of this section is devoted to defining appropriate estimates of the fault magnitudes and analyzing their statistical distributions, so that thresholds for deciding if they are "large" can be set.

Let the overscore symbol "$\hat{\ }$" denote an estimate of a quantity, and the subscript "i" on a vector denote its ith element. For each panel index ($j = 1, 2, \ldots, N$) consider the least squares estimate of $\mathbf{v}(j)$,

$$\hat{\mathbf{v}}(j) = [\mathbf{C}^T\mathbf{C}]^{-1}\mathbf{C}^T\mathbf{x}(\mathbf{j}) \qquad (3.1)$$

Unless $n \gg p$, $\hat{\mathbf{v}}(j)$ may not be a very good estimate of $\mathbf{v}(j)$. However, it will still allow us to estimate the variances of its elements. Define the following estimates of $\{\sigma_i^2\}_{i=1}^p$.

$$\hat{\sigma}_i^2 \equiv \frac{1}{N}\sum_{j=1}^{N} \hat{\mathbf{v}}_i^2(j) \qquad (3.2)$$

It will become apparent shortly that we also require an estimate of σ_w^2, which we define as

$$\hat{\sigma}_w^2 \equiv \frac{1}{N(n-p)}\sum_{j=1}^{N} \hat{\mathbf{w}}^T(j)\hat{\mathbf{w}}(j), \qquad (3.3)$$

where

$$\hat{\mathbf{w}}(j) \equiv \mathbf{x}(j) - \mathbf{C}\hat{\mathbf{v}}(j) \qquad (3.4)$$

is an estimate of $\mathbf{w}(j)$ for $j = 1, 2, \ldots, N$.

The following theorem states the statistical properties of the estimates. Proof is given in the appendix.

Theorem 1: For the model (2.2) under assumptions (A1)–(A3), the estimates of the fault magnitudes (3.2) and noise variance (3.3) have the following statistical properties.

$$(i)\quad \hat{\sigma}_i^2 \sim [\sigma_i^2 + \sigma_w^2[\mathbf{C}^T\mathbf{C}]_{i,i}^{-1}]\frac{\chi^2(N)}{N}, \qquad i = 1, 2, \ldots, p,$$

i.e. $\hat{\sigma}_i^2$ is distributed as a chi-squared random variable multiplied by a constant. $\chi^2(N)$ denotes a chi-squared random variable with N degrees-of-freedom, and $[\mathbf{C}^T\mathbf{C}]_{i,i}^{-1}$ is the ith diagonal element of $[\mathbf{C}^T\mathbf{C}]^{-1}$.

$$(ii)\qquad \hat{\sigma}_w^2 \sim \sigma_w^2\frac{\chi^2(N(n-p))}{N(n-p)}.$$

(iii) $\hat{\sigma}_w^2$ is independent of $\{\hat{\sigma}_i^2\}_{i=1}^p$.

Remark 1 Since the expected value of a χ^2 random variable divided by its degrees-of-freedom is 1, $\hat{\sigma}_i^2$ is a biased estimate of σ_i^2, whereas $\hat{\sigma}_w^2$ is an unbiased estimate of σ_w^2. An unbiased estimated of σ_i^2 would be $\hat{\sigma}_i^2 - \hat{\sigma}_w^2[\mathbf{C}^T\mathbf{C}]_{i,i}^{-1}$.

Remark 2. From (i), if the ith fault is not present ($\sigma_i^2 = 0$), $\hat{\sigma}_i^2$ is a χ^2 random variable multiplied by a positive constant $\sigma_w^2[\mathbf{C}^T\mathbf{C}]_{i,i}^{-1}/N$. If the ith fault is present ($\sigma_i^2 > 0$), $\hat{\sigma}_i^2$ is a χ^2 random variable multiplied by a larger constant. This suggests a χ^2 test on $\hat{\sigma}_i^2$ for detecting the presence of the ith fault, where the threshold of the test is chosen to give a specified probability of false alarm. However, the threshold would depend on the unknown σ_w^2. Substituting $\hat{\sigma}_w^2$ for σ_w^2 provides a solution, but the true probability of false alarm would then not be the desired one and would be difficult to calculate.

In light of Remark 2, we define the test statistics

$$F_i \equiv \frac{\hat{\sigma}_i^2}{[\mathbf{C}^T\mathbf{C}]_{i,i}^{-1}\hat{\sigma}_w^2}, \quad i = 1, 2, \ldots, p. \tag{3.5}$$

The following corollary follows directly from Theorem 1 and the definition of the F-distribution.

Corollary 2 The test statistics $\{F_i\}_{i=1}^p$ defined in (3.5) are distributed as F-distributed random variables multiplied by constants

$$F_i \sim \left[1 + \frac{\sigma_i^2}{[\mathbf{C}^T\mathbf{C}]_{i,i}^{-1}\sigma_w^2}\right]F(N, N(n-p)).$$

$F(\nu_1, \nu_2)$ denotes an F-distributed random variable with ν_1 numerator degrees-of-freedom and ν_2 denominator degrees-of-freedom.

$\sigma_i^2 = 0$ is interpreted as the ith fault not being present, and $\sigma_i^2 > 0$ is interpreted as the ith fault being present. Consequently, it follows from Corollary 2 that if the ith fault is not present, $F_i \sim F(N, N(n-p))$. On the other hand, if the ith fault is present, F_i is distributed as an $F(N, N(n-p))$ random variable scaled by a constant $[1 + \sigma_i^2/[\mathbf{C}^T\mathbf{C}]_{i,i}^{-1}\sigma_w^2] > 1$. Thus, with the ith fault present the distribution of F_i is shifted to the right. An example of how the distribution is shifted is illustrated in Fig. 3.1, where the parameters $n = 6$, $p = 3$, $N = 30$, and $\sigma_i^2/[\mathbf{C}^T\mathbf{C}]_{i,i}^{-1}\sigma_w^2 = 3.85$ have been used.

This suggests using an F-test to detect the presence of each of the p faults. Each of the statistics $\{F_i\}_{i=1}^p$ would be compared to a threshold γ, chosen to provide a specified probability of false alarm. Thus, if α denotes the desired probability of false alarm, γ would be set as the $1-\alpha$ percentile of the $F(N, N(n-p))$ distribution. For each $i \in \{1, 2, \ldots, p\}$, if F_i is larger than γ, it is concluded that the ith fault has occurred. Otherwise, it is concluded that the ith fault has not occurred.

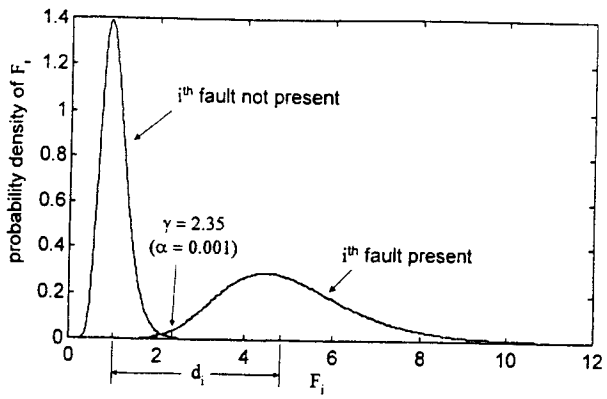

Fig. 3.1 Example illustrating the distribution of a test statistic with and without the corresponding fault present

Remark 3. The validity of Corollary 2 relies on the assumptions regarding the distribution of the underlying random variables. In particular, assumption (A1), which requires that $\mathbf{v}(\cdot)$ is zero-mean. In practice, many locating element faults appear in the data as a mean shift, rather than (or in addition to) a variance change, examples of which are a bent pin or a mislocated pin. If the ith fault occurs and causes the mean of $\mathbf{v}_i(\cdot)$ to become non-zero, then the distribution of F_i is no longer given by Corollary 2. However, the above test, unmodified, can still be successfully applied to detecting the ith fault. The problem must be formulated slightly differently. Define the absence of the ith fault to be that $\mathbf{v}_i(\cdot)$ is zero-mean and has zero variance ($\sigma_i^2 = 0$). Define the presence of the ith fault to be that $\mathbf{v}_i(\cdot)$ has either non-zero mean, non-zero variance, or both. If the ith fault is not present, F_i still follows an $F(N, N(n-p))$ distribution. The threshold for the above test can then be selected, as before, to be the $1-\alpha$ percentile of the $F(N, N(n-p))$ distribution. If the ith fault is present, regardless of whether it causes a mean shift or variance change in $\mathbf{v}_i(\cdot)$, the measurement vectors $\mathbf{x}(\cdot)$ will have larger components along $\mathbf{c}_i$. This will cause $\hat{\sigma}_i^2$ from (3.2), and thus F_i, to be larger on average than if the ith fault were not present. If the fault is large enough, it is likely that F_i will lie above the threshold, signaling that the ith fault has occurred. These intuitive arguments can be rigorously justified by showing that F_i, under the same assumptions as before except that $\mathbf{v}_i(\cdot)$ is no longer required to be zero-mean, follows a noncentral F-distribution. The non-central F-distribution is also shifted to the right relative to the $F(N, N(n-p))$ distribution, in a manner similar to that shown in Fig. 3.1. See Rao (1973) for a discussion on the distribution of quadratic forms of Gaussian random variables and the noncentral F-distribution. Once the ith fault is detected, whether it was a mean shift or variance change can easily be determined by inspecting $\{\hat{\mathbf{v}}_i(j)\}_{j=1}^N$ and determining if they have experienced a mean shift or variance change.

Remark 4 Another violation of the assumptions that would cause the distribution of F_i to differ from that of Corollary 2, is if $\mathbf{v}(\cdot)$ was nonstationary. If no fault is present, $\mathbf{v}(\cdot)$ is stationary by definition, since it is assumed identically zero. However, suppose the ith fault is present and that, instead of σ_i^2 being constant over the data window of N panels, it grows slowly. The distribution of F_i is no longer given by Corollary 2, and its exact distribution is intractable. Regardless, by the same reasoning outlined in Remark 3, $\mathbf{x}(\cdot)$ will have larger components along $\mathbf{c}_i$ than if the ith fault were not present, and F_i will likely signal an alarm. Once the ith fault is detected, $\{\hat{\mathbf{v}}_i(j)\}_{j=1}^N$ can again be inspected to determine if the fault magnitude is growing or steady.

3.2 Discussion. As illustrated in Fig. 3.1, the probability of detecting the ith fault (of a given magnitude) is the area to the right of γ under the distribution with the fault present. This probability depends on how much the distribution is shifted over when the fault is present, which, from Corollary 2, depends solely on the quantity

$$d_i \equiv \frac{\sigma_i^2}{[\mathbf{C}^T\mathbf{C}]^{-1}_{i,i}\sigma_w^2}, \quad i = 1, 2, \ldots, p. \tag{3.6}$$

d_i, which we will refer to as the detectability index for the ith fault, is closely related to what can be interpreted as a signal-to-noise ratio. In order to define a signal-to-noise ratio, we first define the following measure of the average variance of the n measurement points:

$$\bar{\sigma}^2 \equiv \frac{\sum_{j=1}^{n} \text{Var}\,[\mathbf{x}_j(\cdot)]}{n}. \tag{3.7}$$

It can be shown that if the ith fault (but no other fault) is present, then

$$\bar{\sigma}^2 = \frac{\sigma_i^2}{n} + \sigma_w^2. \tag{3.8}$$

Thus, the portion of the average variance of the measurement points due to the ith fault is σ_i^2/n, and the portion due to the inherent noise is σ_w^2. Consequently, a signal-to-noise ratio for the ith fault can be defined as

$$\text{SNR}_i \equiv \frac{\sigma_i^2}{n\sigma_w^2}. \tag{3.9}$$

If the columns of $\mathbf{C}$ are not too close to being linearly dependent, $[\mathbf{C}^T\mathbf{C}]^{-1}_{i,i}$ should lie in the neighborhood of 1. Note that if the columns of $\mathbf{C}$ are orthogonal or if $p = 1$, $[\mathbf{C}^T\mathbf{C}]^{-1}_{i,i}$ is identically 1. Consequently, the detectability index for the ith fault is approximately n times the signal-to-noise ratio for the ith fault, i.e.

$$d_i \cong n\text{SNR}_i. \tag{3.10}$$

From (3.10) it is apparent that the detectability of a fault depends strongly on its signal-to-noise ratio. At first glance, the factor n in (3.10) appears to cancel out the n in the denominator of (3.9). However, the columns of $\mathbf{C}$ are always scaled to have unit norm. Consequently, as the number of measurement points n increases, the magnitude of the elements of $\mathbf{c}_i$ must be decreased—roughly by a factor of $\sqrt{n}$. In the model (2.2), this must be compensated for by increasing σ_i by the same factor, even though the size of the fault has not changed. The net result is that σ_i^2 increases roughly proportionally to n, and the signal-to-noise ratio is approximately independent of n. Thus, from (3.10) the detectability of a fault also depends strongly on the number of relevant measurement points.

A main advantage of the method presented in this section over PCA is that the least squares based method developed here can detect and classify multiple faults. F_i is the test statistic used to detect the ith fault. From Corollary 2, the distribution of F_i depends on the presence of the ith fault (i.e. on σ_i^2) and is independent of the presence of any of the other modeled faults. Thus, the ability of the test to detect a particular fault is not affected by the presence of any of the other faults. In contrast, the PCA-based method of Ceglarek and Shi (1996) can only be applied to detecting single fixture faults.

Another main advantage over PCA is that the probability distribution of the test statistics are of very simple form. The result of this is that γ can be easily chosen to provide a desired probability of false alarm, and the probability of detecting faults can be easily calculated. Calculation of these probabilities requires only F-distribution tables, which are widely available. Moreover, if $F_\alpha(\nu_1, \nu_2)$ denotes the $1 - \alpha$ percentile of the $F(\nu_1, \nu_2)$ distribution, the following approximations are quite close for $\nu_1 \geq 10$ and $\nu_2 \geq 30$ (Bowker and Liebermann, 1961):

$$\log_{10} F_{0.001}(\nu_1, \nu_2) \cong \frac{2.6841}{\sqrt{h - 2.09}} - 1.672\left(\frac{1}{\nu_1} - \frac{1}{\nu_2}\right),$$

$$\log_{10} F_{0.005}(\nu_1, \nu_2) \cong \frac{2.2373}{\sqrt{h - 1.61}} - 1.250\left(\frac{1}{\nu_1} - \frac{1}{\nu_2}\right),$$

and

$$\log_{10} F_{0.01}(\nu_1, \nu_2) \cong \frac{2.0206}{\sqrt{h - 1.40}} - 1.073\left(\frac{1}{\nu_1} - \frac{1}{\nu_2}\right),$$

where $h \equiv 2/(1/\nu_1 + 1/\nu_2)$. In the PCA method of Ceglarek and Shi (1996), the distributions of the test statistics are highly complicated and completely unknown. Thus, threshold selection is not straightforward, and very little analysis of probabilities of detection and false alarm can be made other than through Monte Carlo simulation.

An additional feature of the algorithm of this paper is that it is well suited for sequential detection. That is, as the $(N + 1)^{st}$ panel is measured, estimate $\hat{\mathbf{v}}(N + 1)$ and $\hat{\mathbf{w}}(N + 1)$ and update $\hat{\sigma}_w^2$, $\{\hat{\sigma}_i^2\}_{i=1}^p$, and $\{F_i\}_{i=1}^p$. Note that, to provide the desired probability of false alarm, γ must also be updated based on the $F(N + 1, (N + 1)(n - p))$ distribution. If implemented in this manner, the process can be monitored from the first panel produced, allowing early detection of the fault (if its magnitude is sufficiently large).

4 Theoretical Analysis

As mentioned in the preceeding section, one advantage of the detection algorithm of this paper is that its performance, in terms of probabilities of false alarm and detection, can easily be determined analytically. In this section, we analyze the algorithm performance for the situation illustrated in Fig. 2.1 and Fig. 2.2.

The faults considered are P_1 variations in the x and z directions and P_2 variation in the z direction ($p = 3$). $\mathbf{x}(\cdot)$ consists of the deviations from nominal of the x-y-z coordinates of the three measurement points, M_1, M_2, and M_3 ($n = 9$). The nominal x-y-z coordinates for P_2 and the measurement points are $P_2 = (6, 0, 0)$, $M_1 = (-1, 0, -1)$, $M_2 = (7, 0, -1)$, and $M_3 = (7, 0, 4)$, where the origin of the coordinate system coincides with P_1. From the geometry of the panel and tooling, $\mathbf{C}$ was found to be

$$\mathbf{C} = \begin{bmatrix} .093 & .577 & -.120 \\ 0 & 0 & 0 \\ -.093 & 0 & .843 \\ .093 & .577 & -.120 \\ 0 & 0 & 0 \\ .647 & 0 & -.120 \\ -.370 & .577 & .482 \\ 0 & 0 & 0 \\ .647 & 0 & -.120 \end{bmatrix},$$

where the first column corresponds to P_2 variation in the z direction (fault 1), and the second and third columns correspond to P_1 variation in the x (fault 2) and z (fault 3) directions, respectively. Note that the diagonal elements of $[\mathbf{C}^T\mathbf{C}]^{-1}$ are $[\mathbf{C}^T\mathbf{C}]^{-1}_{1,1} = 1.24$, $[\mathbf{C}^T\mathbf{C}]^{-1}_{2,2} = 1.02$, and $[\mathbf{C}^T\mathbf{C}]^{-1}_{3,3} = 1.25$.

The probability of detecting fault 1 for various sample sizes (N) and various signal-to-noise ratios was calculated analytically using Corollary 1, and the results are plotted in Fig. 4.1. For all sample sizes the threshold γ, which depends on N, was chosen to provide a probability of false alarm $\alpha = 0.001$. Even

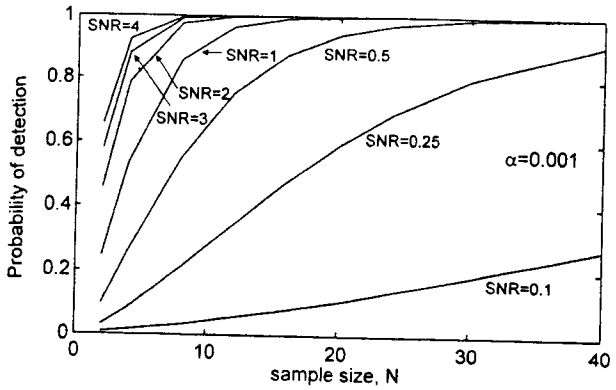

Fig. 4.1 Example probability of detection curves for a $P_2(z)$ fault with various signal-to-noise ratios and sample sizes. Probability of false alarm was set at 0.001.

for small signal-to-noise ratios, such as SNR = 0.25, the probability of detecting fault 1 is high with a sample size of 40 panels. For large signal-to-noise ratios, the probability of detection is close to 100% after only a few panels are measured. With identical SNR's, any difference in the probability of detection for the different faults must result from differences in the corresponding diagonal elements of $[\mathbf{C}^T\mathbf{C}]^{-1}$ (see Corollary 2). Since the diagonal elements are similar for all three faults, the detection results for faults 2 and 3 are very similar to those for fault 1 and are not shown. The detection results for fault 2 are, in fact, slightly better than for fault 1, since $[\mathbf{C}^T\mathbf{C}]^{-1}_{2,2}$ is smaller than $[\mathbf{C}^T\mathbf{C}]^{-1}_{1,1}$.

5 Experimental Results

This section presents experimental results for applying the algorithm to fixture diagnosis in autobody panel assembly. Figure 5.1 shows the points that are measured on the right-hand bodyside. Both the x- and z-directions of Points M_1 through M_4 are measured. The x-direction of points M_5 through M_8 and the z-direction of points M_9 and M_{10} are also measured. A similar measurement scheme is used for the left-hand bodyside. The z-direction is upwards, and the x-direction is towards the rear of the vehicle. The measurements are taken after the framing station, in which the left and right bodysides are joined to the underbody and roof. Pins P_1 and P_2 locate the bodyside in the x-z plane at the framing station, P_1 mating with a hole in the bodyside and P_2 mating with a slot. The goal is to detect fixturing errors in the framing station due to P_1 and P_2 faults.

Although the bodyside is rigid in the x-z plane, it is not completely rigid in the y-direction. Consequently, more than three blocks are used to constrain the bodyside position in the y-direction. These blocks, which are not shown in Fig. 5.1, are positioned in such a way that the x-z plane is a "slip" plane, i.e. locating error in the x-z plane due to P_1 and P_2 faults does not cause locating error in the y direction. Thus, for the purpose of simplifying the analysis, attention was focused on P_1 and P_2 faults, and all y-direction measurements have been ignored.

The nominal x-z coordinates of the pins and measurement points are shown in Table 5.1. The 14-dimensional measurement vector for each autobody is defined as $\mathbf{x}(\cdot) \equiv [M_1(x)\ M_2(x) \ldots M_8(x)\ M_1(z)\ M_2(z)\ M_3(z)\ M_4(z)\ M_9(z)\ M_{10}(z)]^T$. Two fixture faults will be considered: a P_1 failure in the x-direction (fault 1) and a P_2 failure in the z-direction (fault 2). Note that fault 1 causes a translation in the x-direction and fault 2 causes a rotation about P_1. From the panel geometry (i.e., the nominal coordinate data in Table 5.1) and the definition of $\mathbf{x}(\cdot)$, it follows that the fault matrix is

$$\mathbf{C} = \begin{bmatrix} 0.354 & 0.057 \\ 0.354 & -0.026 \\ 0.354 & 0 \\ 0.354 & -0.004 \\ 0.354 & 0.046 \\ 0.354 & -0.087 \\ 0.354 & -0.024 \\ 0.354 & 0.043 \\ 0 & 0.187 \\ 0 & 0.361 \\ 0 & 0 \\ 0 & 0.535 \\ 0 & 0.495 \\ 0 & 0.536 \end{bmatrix}.$$

The results of the fault detection algorithm, applied recursively to a total of 14 measured autobodies, are shown in Fig. 5.2. As each new autobody was measured, the sample size N from which the test statistics are calculated increased by one. Thus, the parameters for the algorithm were $n = 14$ (14 measurements per autobody) and $p = 2$ (2 faults tested for), with N increasing from 1 to 14. The threshold γ was selected to provide a probability of false alarm of 0.001. Specifically, for each value of N, γ was chosen to be the 0.999 percentile of the $F(N, 12N)$ distribution. As N increases, γ decreases, as illustrated in Fig. 5.2.

Figure 5.2 shows that F_1 crossed the threshold when the second autobody was measured and afterwards remained significantly above the threshold. In contrast, F_2 remained significantly below the threshold. The results indicated that fault 1 (P_1 failure in the x-direction) was strongly present and fault 2 was absent. Further investigation of the framing station revealed that fault 1 had, indeed, occurred. Through extended use, pin

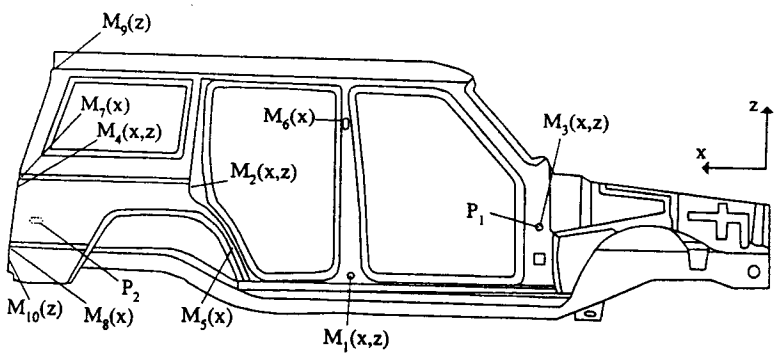

Fig. 5.1 Key points on the right-hand bodyside. M_1 through M_{10} are points measured on the bodyside after the framing station, where the letters in parentheses indicate the directions(s) that are measured. P_1 and P_2 are pins that locate the bodyside in the x-z plane at the framing station.

Table 5.1 Nominal x-z coordinates for measurement points and pins

point	nominal coordinates (mm)	
	x	z
M_1	3134	1200
M_2	4015	1618.5
M_3	2184	1489
M_4	4895.3	1510.5
M_5	3721	1256.5
M_6	3264	1930
M_7	4895	1608
M_8	4895.5	1273
M_9	4693.8	2228.5
M_{10}	4899	1214.5
P_1	2184	1489
P_2	4680	1428

P_1 had become worn so that its diameter in the x-direction was approximately 2.5 mm smaller than nominal. This caused the bodysides to shift back and forth in the x-direction as they were placed in the framing station fixture. P_1 was subsequently replaced, and the problem was eliminated.

6 Conclusions

In this paper, a method for diagnosing fixture related faults in panel assembly was developed. The faults considered are panel positioning errors resulting from worn, damaged, or mislocated locating elements. A model relating the fixture faults to the displacement of measured points on the panels was presented and used to develop a least squares based algorithm for detecting and classifying multiple faults. Implementation of the algorithm requires off-line product/process design information regarding the geometry of the panel and fixture (used to construct the fault model) and in-line dimensional measurements obtained, for example, with an OCMM.

The algorithm has a number of advantages over existing algorithms for fixture diagnosis. Specifically, the algorithm of this paper can detect and classify multiple fixture faults and amounts to an F-test that is both easily implemented and analyzed. Due to the simplicity of the test and the well known properties of the F-distribution, the test performance (in terms of probability of detecting faults and probability of false alarm) can be completely determined off-line and used to easily and reliably select the test threshold to ensure a desired probability of false alarm. Moreover, there exists a clear physical interpretation of the detectability of the faults, in terms of their signal-to-noise ratios. The test performance for a 3-2-1 rigid body fixturing example was analyzed theoretically, demonstrating that the test has excellent detection capabilities. The performance was also verified experimentally by applying it to fixture fault detection in autobody panel assembly.

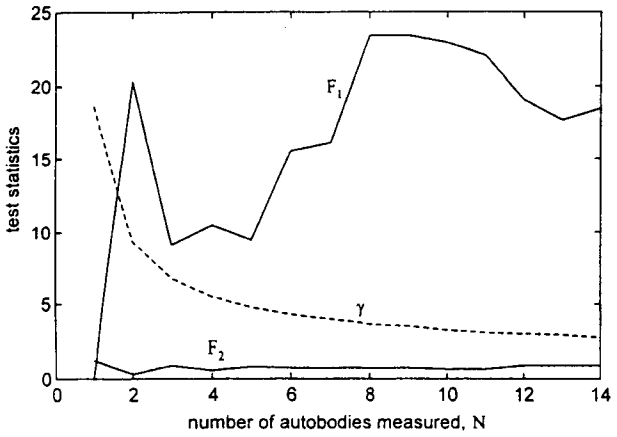

Fig. 5.2 Experimental results for detection of two potential faults in autobody panel assembly (fault 1 was present; fault 2 was not)

Extensions of the method to other types of tooling failures are being investigated. Specifically, dimensional variation due to misaligned weld guns and clamps are under consideration. The effect of such failures is a resultant force applied to the panel at the location of the failing tooling element. If the effects of such forces on the panel deformation can be linearized and put into the form of (2.2), then the model and algorithm developed in this paper may be applicable to these types of tooling failures as well.

References

ABC, 1993, "Variation Reduction for Automotive Body Assembly," *Annual Report for Advanced Technology Program (NIST)*, Autobody Consortium and The University of Michigan, Ann Arbor.

Asada, H., and By, A., 1985, "Kinematic Analysis of Workpart Fixturing for Flexibly Assembly with Automatically Reconfigurable Fixtures," *IEEE Journal of Robotics and Automation*, Vol. RA-1, No. 2, pp. 86–94.

Bowker, A., and Lieberman, G., 1961, *Handbook of Industrial Statistics*, Prentice-Hall, Englewood Cliffs, NJ.

Ceglarek, D., Shi, J., and Wu, S. M., 1994, "A Knowledge-based Diagnosis Approach for the Launch of the Auto-body Assembly Process," ASME JOURNAL OF ENGINEERING FOR INDUSTRY, Vol. 116, No. 3, pp. 491–499.

Ceglarek, D., and Shi, J., 1996, "Fixture Failure Diagnosis for Autobody Assembly Using Pattern Recognition," ASME JOURNAL OF ENGINEERING FOR INDUSTRY, Vol. 118, No. 1, pp. 55–66.

Chou, Y., Chandru, V., and Barash, M., 1989, "A Mathematical Approach to Automatic Configuration of Machining Fixtures: Analysis and Synthesis," ASME JOURNAL OF ENGINEERING FOR INDUSTRY, Vol. 111, Nov., 1989, pp. 299–306.

De Meter, E., 1995, "Min-Max Load Model for Optimizing Machining Fixture Performance," ASME JOURNAL OF ENGINEERING FOR INDUSTRY, Vol. 117, May, 1995, pp. 186–193.

Hockenberger, M., and De Meter, E., 1995, "The Effect of Machining Fixture Design Parameters on Workpiece Displacement," *Manufacturing Review*, Vol. 8, No. 1, pp. 22–32.

Hu, S., and Wu, S. M., 1992, "Identifying Root Causes of Variation in Automobile Body Assembly Using Principle Component Analysis," *Transactions of the NAMRI*, Vol. XX, pp. 311–316.

King, L., and Hutter, I., 1993, "Theoretical Approach for Generating Optimal Fixturing Locations for Prismatic Workparts in Automated Assembly," *Journal of Manufacturing Systems*, Vol. 12, No. 5, pp. 409–416.

Menassa, R., and DeVries, W., 1991, "Optimization Methods Applied to Selecting Support Positions in Fixture Design," ASME JOURNAL OF ENGINEERING FOR INDUSTRY, Vol. 113, Nov., 1991, pp. 412–418.

Rao, C., 1973, *Linear Statistical Inference and Its Applications, 2nd edition*, Wiley, New York, NY.

Rong, Y., and Zhu, Y., 1992, "Application of Group Technology in Computer-aided Fixture Design," *International Journal of Systems Automation: Research and Applications*, Vol. 2, No. 4, pp. 395–405.

Rong, Y., Li, W., and Bai, Y., 1995, "Locator Error Analysis for Fixturing Accuracy Verification," *Proc., ASME International Computers in Engineering Conference*, Boston, MA., pp. 825–832.

APPENDIX

The proof of Theorem 1 is provided in this appendix. Substituting (2.2) into (3.1) gives

$$\hat{\mathbf{v}}(j) = \mathbf{v}(j) + [\mathbf{C}^T\mathbf{C}]^{-1}\mathbf{C}^T\mathbf{w}(j)$$

$$\sim N(\mathbf{0}, \mathbf{K}_v + \sigma_w^2[\mathbf{C}^T\mathbf{C}]^{-1}), \quad \text{(A1)}$$

since $\mathbf{v}(j)$ is assumed independent of $\mathbf{w}(j)$. Thus, the ith element of $\hat{\mathbf{v}}(j)$ follows the normal distribution

$$\hat{\mathbf{v}}_i(j) \sim N(0, \sigma_i^2 + \sigma_w^2[\mathbf{C}^T\mathbf{C}]_{i,i}^{-1}), \quad \text{(A2)}$$

and its square is a chi-squared random variable multiplied by a constant

$$\hat{\mathbf{v}}_i^2(j) \sim [\sigma_i^2 + \sigma_w^2[\mathbf{C}^T\mathbf{C}]_{i,i}^{-1}]\chi^2(1). \quad \text{(A3)}$$

Since $\mathbf{v}(j)$ and $\mathbf{w}(j)$ are assumed independent of $\mathbf{v}(i)$ and $\mathbf{w}(i)$ for $i \neq j$,

$$\hat{\sigma}_i^2 \equiv \frac{1}{N}\sum_{j=1}^{N} \hat{\mathbf{v}}_i^2(j) \sim [\sigma_i^2 + \sigma_w^2[\mathbf{C}^T\mathbf{C}]_{i,i}^{-1}] \frac{\chi^2(N)}{N} \quad \text{(A4)}$$

by the reproductive property of the chi-squared distribution, and (i) is proven.

Substituting (2.2) and (A1) into (3.4) gives

$$\hat{\mathbf{w}}(j) = [\mathbf{I} - \mathbf{C}(\mathbf{C}^T\mathbf{C})^{-1}\mathbf{C}^T]\mathbf{w}(j), \quad \text{(A5)}$$

which implies

$$\hat{\mathbf{w}}^T(j)\hat{\mathbf{w}}(j) = \mathbf{w}^T(j)[\mathbf{I} - \mathbf{C}(\mathbf{C}^T\mathbf{C})^{-1}\mathbf{C}^T]\mathbf{w}(j) \sim \sigma_w^2\chi^2(n-p). \quad \text{(A6)}$$

(A6) follows from the Fisher-Cochran Theorem (Rao, 1973), since the matrix in brackets is both symmetric and idempotent with rank $n - p$. Again, by the reproductive property of the chi-squared distribution and the definition of $\hat{\sigma}_w^2$, (ii) follows.

To prove (iii) first note that, from (A1) and (A5), $\hat{\mathbf{v}}(j)$ and $\hat{\mathbf{w}}(j)$ are both zero-mean and Gaussian and $\hat{\mathbf{v}}(j)$ is independent of $\hat{\mathbf{w}}(i)$ for $i \neq j$. $\hat{\mathbf{v}}(j)$ is also uncorrelated with $\hat{\mathbf{w}}(j)$ since, using (A1) and (A5),

$$E[\hat{\mathbf{w}}(j)\hat{\mathbf{v}}^T(j)] = E\{[\mathbf{I} - \mathbf{C}(\mathbf{C}^T\mathbf{C})^{-1}\mathbf{C}^T]\mathbf{w}(j)[\mathbf{v}^T(j) + \mathbf{w}^T(j)\mathbf{C}(\mathbf{C}^T\mathbf{C})^{-1}]\}$$
$$= [\mathbf{I} - \mathbf{C}(\mathbf{C}^T\mathbf{C})^{-1}\mathbf{C}^T]E[\mathbf{w}(j)\mathbf{v}^T(j)] + \sigma_w^2[\mathbf{I} - \mathbf{C}(\mathbf{C}^T\mathbf{C})^{-1}\mathbf{C}^T]\mathbf{C}(\mathbf{C}^T\mathbf{C})^{-1} = \mathbf{0}.$$

Since $\hat{\mathbf{v}}(j)$ and $\hat{\mathbf{w}}(j)$ are Gaussian and uncorrelated, they are independent. Thus, $\hat{\mathbf{v}}(j)$ and $\hat{\mathbf{w}}(i)$ are independent for all i and j, which implies (iii).